Journal of Hydraulic Structures
J. Hydraul. Struct., 2020; 6(1): 55-76
DOI: 10.22055/jhs.2020.32753.1134

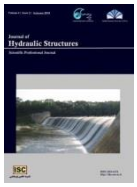

Experimental and numerical investigation the effect of pier position on local scouring around bridge pier at a 90° convergent bend

Mousa Rasaei[1]
Sohrab Nazari[1,2]
Saeid Eslamian[1,3]

Abstract

Natural rivers have several bends along the path that are not generally uniform and some are convergent. Installing the bridge piers in river convergent bends may result in complicated flow and erosion patterns around the bridge piers. Most of previous studies on the flow and the scour pattern around piers were carried out in straight channels and fixed-width bends. Studying the local scouring around pier located at a converging bend, experimentally and numerically, has brought novelty to this paper. In this research, a physical hydraulic model with a 90° convergent bend and central radius of 170 cm was built. A cylindrical pier with a diameter of 60 mm was installed in positions of 0, 30, 45, 60, and 75 degrees and local scour were studied under clear-water conditions. The SSIIM-2 numerical model was also used to simulate the scour pattern and the results were compared with experimental results. The results showed that, increasing the convergence and changing the pier position in a bend leads to an increment in the continuity between the flow lines and secondary currents, respectively, so that the maximum depth and volume of the scour hole occurred in the second half of the bend at an angle of 75 degrees. The comparison between experimental and numerical data shows that SSIIM-2 model can efficiently simulate the scour pattern in a 90° convergent bend. Furthermore, in all cases by increasing the Froude number, maximum depth and volume of the scour hole were increased.

Keywords: Bridge pier; pier position; local scouring; 90° convergent bend; the SSIIM-2 numerical model.

Received: 27 February 2020; Accepted: 15 March 2020

[1] Department of Civil Engineering, Najafabad Branch, Islamic Azad University, Najafabad, Iran.
[2] Department of Civil Engineering, Eqhlid Branch, Islamic Azad University, Eqhlid, Iran. **(Corresponding author)**
[3] Department of Water Engineering, Isfahan University of Technology, Isfahan, Iran.

1. Introduction

Rivers are the main vital elements of human societies that have several bends in their long paths. The mechanism of scouring process and the hydrodynamics of flow around bridge piers in a river bend are of great importance to engineers and researchers in the field of environmental fluid mechanics and ecology [1]. In the river bends, the interaction of the transverse pressure gradient and the centrifugal force forms the secondary currents. The presence of secondary currents in a river bend brings the movement of sedimentary materials from the outer bend to the inner bend. This leads to the accumulation of sediments, followed by width reduction of the bend and eventually convergence in the bend (Fig. 1). Due to integration of secondary currents and the main flow, the helical flow is formed in the bend, so that this helical flow plays a main role in the formation and development of bed changes and distribution of shear stress at the bottom of the channel [2].

Bridges are one of the most significant and beneficial river structures and large number of them are destroyed yearly due to the scouring and erosion phenomenon. During road construction and lack of river stability, bridge piers may be placed in the river convergent bends. So that affects the helical flow and adds to the complexity of the flow behavior. In addition, the bridge piers in the flow path leads to a change in the flow structure and formation of vortices system around the bridge piers. This system consists of a horseshoe vortex initiated by the down flow at the upstream face of the pier, and wake vortices which shed from sides of the pier due to flow separation [3]. These vortices were introduced as the main factors of scouring around the bridge piers (Fig 2).

Figure 1. Illustration of a natural river with a convergent bend

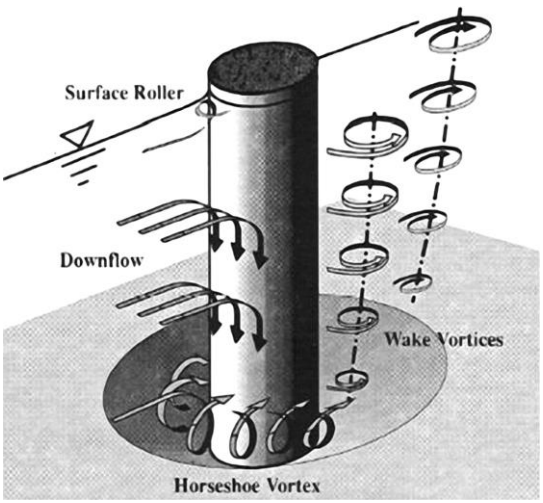

Figure 2. Flow and scour pattern around a cylindrical pier [4]

In recent years, many researchers have conducted experimental and numerical studies on the flow and scour patterns around bridge piers in straight and bend channels, Shukry [5] is the earliest. He performed some tests in 90° and 180° bends in rectangular channels with different values for ratio of width to flow depth and ratio of radius of the bend to flow width. Rozovskii [2] studied the flow pattern and boundary shear stress distribution in channel bends with a fixed bed. Booij [6] modeled the structure of the secondary flow in a 180° fixed-width bend and found that the secondary flow increases local scouring in the outer wall. The effect of different types of

cohesive soil on the scour around a single, vertical pier located at a straight channel was investigated by Najafzadeh and Barani [7]. Blanckaert and Graf [8] studied the flow pattern in a mild 120 degrees bend in a channel. Wildhagen [9] studied the sediment transport in channels with sharp bends by using the SSIIM numerical model. He concluded that capability of SSIIM model has led to its popularity in hydraulics engineering, and is used as a model appropriate for studying and designing sediment and flow pattern. Vaghefi et al. [10] conducted a set of experiments on the scour around a triple cylindrical pier series in two positions, perpendicular to the flow and with stream wise direction, under clear water conditions in a laboratory flume with a 180° sharp bend. Their results demonstrated that the maximum scour depth occurred in the case of installing the piers perpendicular to the flow at the 90° position. Georgiadou and Smith [11] were one of the pioneers in the field of flow hydraulics in convergent bends. Based on the status of the flow pattern and a physical model with a 90° convergent bend, they revealed that under convergent conditions of the bend, the maximum velocity path is located near the inner bend. Tabarestani et al. [12] experimentally analyzed the effect of different sizes of riprap on the scour around rectangular bridge piers in the presence or absence of a collar. Ghodsian and Mousavi [13] discovered the correlation between the maximum scour depth in a channel bend and the densimetric Froude number, relative bend radius and relative depth of flow. Recently, Ghobadian and Mohammadi [14] used the SSIIM 3-D numerical model to investigate flow characteristics in a 180° convergent bend. Their results indicated that in a convergent channel, the maximum velocity path at a plane near the water surface crosses the channel's centerline at about a 30° to 40° cross-section, while in the uniform bend, this occurs at about the 50° cross-section. Mansuri [15] studied the over-time bed evolution in 180° river bends with the SSIIM 3-D model. Gholami et al. [16] used experimental and numerical models to show that the maximum velocity in a sharp bend remained at the inner channel wall until the final section, and the maximum velocity was transmitted to the outer channel wall in sections beyond the bend. Abdallah Mohamed et al. [17] reported that the SSIIM numerical model has high ability to simulate local scouring at bridge pier. Akib et al. [18] simulated the extent of scour as well as the maximum scour depth around bridge piers existing in nature by using SSIIM-2. Ehteram and Meymand [19] also used the SSIIM-2 numerical model to simulate the scour depth at side piers of the bridge. Outputs showed that this model predicts the bed variation and scour depth and it shows the maximum of scour depth but the depth of scour hole is about fifteen percent less than experimental results. Hamidi and Siadatmousavi [20] employed SSIIM numerical model in order to conduct a numerical simulation of the flow pattern and scour around bridge piers. As suggested, they suggested, although SSIIM numerical model was successful in estimating the scour hole at the foot of the adjacent piers, the scour depth between the piers was overestimated. Emami et al. [21] examined the scour around the cylindrical pier in a straight channel and in a U-shape channel. The results showed that the minimum and the maximum scour depth per each discharge occur at straight channel and a section with 60° of bend, respectively. Masjedi et al. [22] studied scour around a rectangular bridge pier at different angles of a 180° bend. As suggested by the results of their study, when the bridge piers are located at the 60° angle from the beginning of the bend, the maximum local scour occurs around the pier. Wang et al. [23] utilized a free flow channel to investigate the local scouring around the paired cylindrical piers in clear water conditions. The results demonstrated that the local scouring depth around the low-stream pier is less than the upstream one. Khajeh et al. [24] investigated the scour pattern around the inclined cylindrical pier located at a 180° fixed-width bend utilizing an experimental model. They figured out that the maximum and minimum scour depth around an inclined pier occurs on the outer and inner sides of the bend, respectively.

Literature review reveals that researchers are mostly focused on flow pattern and scouring around bridge piers located at straight path and sometimes in uniform and fixed-width bends. By reviewing the previous works, a gap related to experimental or numerical analysis on local scouring around piers in convergent bends was seen. The novelty of this study is perhaps related to the experimental and numerical studies for investigating the local scouring around pier located at a converging bend.

In this research, the effect of pier position at different angles of a 90° convergent bend on local scouring around a cylindrical bridge pier was studied under clear-water conditions, experimentally and numerically. The SIIMM 2 numerical model was employed for the simulation. Finally, in order to achieve a better understanding of flow and scour pattern around pier in convergent channels, the experimental results were compared with numerical results and validation was done.

2. Materials and methods

2.1. Dimensional analyses

Numerous parameters are effective on local scour around bridge piers. Important parameters such as; pier characteristics, channel geometry, sediment properties, flow conditions, fluid properties and time. Accordingly, this research has shown the most important parameters in Eq. (1).

$$f_1\left(ds, L, D, V, \upsilon, \theta, g, d_{50}, y, t, \rho, \rho_s, R_C, S_0\right) \quad (1)$$

In which, ds is the maximum scour depth, L is length of pier, D is diameter of pier, V is the approach flow velocity, υ is dynamic viscosity, θ is location of pier in bend, g is gravitational acceleration, d_{50} is median grain size, y is the approach flow depth, t is equilibrium time of scour, ρ is density of water, ρ_s is density of sediment particles, Rc is central radius of bend and S_0 is bed slope. Which by using dimensional analysis and the Buckingham theory, can be written Eq. (2) as below.

$$f_2\left(\frac{d_s}{y}, \frac{L}{y}, \frac{D}{y}, \frac{\upsilon}{vy}, \theta, S_0, t, \frac{gy}{V^2}, \frac{d_{50}}{y}, \frac{TV}{y}, \frac{\rho_s}{\rho}, \frac{R}{y}\right) \quad (2)$$

In which $\frac{\upsilon}{vy}$ represents the effect of the viscous force (reverse Reynolds number), $\frac{gy}{V^2}$ is reverse Froude number. After simplification and eliminating the parameters with constant values in above equation and finally, Eq. (3) presents. In fact, the Eq. (3) is, dimensionless relationship for the maximum relative scour depth (ds/y) as follows:

$$\frac{d_s}{y} = f_3(\theta, Fr) \quad (3)$$

In which, Fr Froude number and θ pier location are considered as final variables.

2.2. Experimental Setup and Procedure

2.2.1. Experimental model

The channel used in this study is located at the hydraulic laboratory of Islamic Azad University of Eghlid, Iran (Fig. 3). The wall and bed of the flume were made of Plexiglas with roughness coefficient of 0.0001. The main channel consisted of a 4.5 m long upstream and a 2 m long downstream straight reaches. A 90° bend with variable width changing from 60 cm at the beginning to 30 cm at the end (convergence ratio of 0.5), which became convergent, was located between the two straight reaches. The central radius of bend was 170 cm and the channel's height were 40 cm. Furthermore, there was a drain valve to set the water level. The water was also pumped by a 5-inch centrifuge pump to the primary reservoir of the main channel through a magnetic flowmeter. After passing through the main channel and the bend section, it goes into two successive reservoirs. A standard trapezoidal nozzle with a width of 20 cm was also used to read the flow rate at the end of the second reservoir.

The size of pier in this research was considered to meet the criteria which have been defined by other investigators [25, 26, 27]. Therefore, in this research the cylindrical pier with diameter of 60 mm fabricated from iron was used. The bed sediments consisted of a 15 cm layer of uniform sand, with median diameter D50 = 1 mm, standard deviation 1.23 and specific gravity of 2.65 gr/cm3, which covered total length of flume [25, 28]. Also, the water depth was fixed at 10 cm in all tests [29].

Figure 3. Laboratory physical model with a 90° convergent bend

2.2.2. Experimental procedures

In the first phase, in order to calibrate the model and establish the condition of clear-water during the experiments, a test was performed without a pier. The sediments with D50 = 1 mm and a thickness of 15 cm spread across the channel. Considering the constant depth of 10 cm for

water along the channel and the maximum discharge required for clear-water conditions was estimated as 11.2 L/S.

Next, to achieve the equilibrium time of the experiments, a long time experiment with the duration of 12 hours was conducted with discharge of 11.2 L/S and the pier was placed at the position of 75°. As shown in Figure 5, approximately 95% of scouring occurs during the first 150 minutes. Therefore, in all experiments, the scour was recorded 150 minutes after the start of each test and was considered here as the maximum scour depth (Fig. 4).

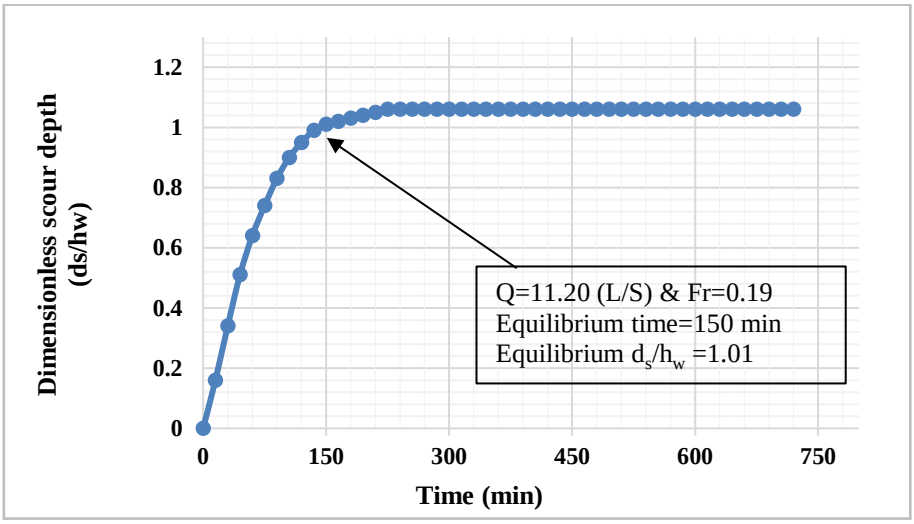

Figure 4. Equilibrium time in the position of 75°

To conduct experiments, a pier was installed at the desired position initially. Before each test the bed sediments were spread extensively throughout the flume and particularly in the vicinity of the pier. To start the test, the end valve was closed and clear water was slowly led into the channel to prevent the formation of ripples and roughness at the bed surface. In the next step, the flow depth of 10 cm and the desired flow rate and clear water conditions were achieved with precise adjustment of the pump, valve and the lower gate. At the completion of each test and after 150 minutes (equilibrium time), the pump was stopped and the flume was drained slowly without disturbing the scour topography. After complete drying of the bed, the maximum scour depth was measured using a depth gauge with a precision of millimeters. Moreover, the bed topography was taken at intervals of 1 cm in the longitudinal, crosswise and altitudinal directions (x,y,z) using a laser meter. Ultimately, the geometry and volume of the scour hole were plotted and calculated using the Surfer software (version 13.5.583). The same conditions were applied for different positions. The pier was installed in positions of 0, 30, 45, 60, and 75 degrees and for discharge rates of 6.10, 8.23, and 11.20 L/S the scour status in clear-water conditions was studied. In total, 15 experiments were carried out for cylindrical pier in different positions according to Table 1.

Table 1. Range of differences and measurable parameters

Effective parameters	Range of differences
Pier Type and Dimensions	Cylindrical pier with diameter of 60 mm
Pier material	Metal
Pier position	0, 30, 45, and 75 degrees
Flow discharge rate	6.10, 8.23, and 11.20 L/S
Froude number	0.1, 0.14 and 0.19
Flow depth	100 mm
Median grain size of bed	1 mm
Roughness coefficient	0.0001
Average thickness of bed particles	150 mm
Density	1 gr/cm^3
geometric standard deviation	1.23
Specific gravity of bed particles	2.65 gr/cm^3

2.3. Mathematical model and methods

2.3.1. The Numerical Model

The SSIIM model (Sediment Simulation in Intakes with Multi-block option) is a three-dimensional model for flow of water and sediment. The first version was introduced at 1993 by Olsen [30] from the school of hydraulic and environmental engineering at Norwegian University of Science and Technology. This model is based on three-dimensional computational fluid dynamics which solves Navier-Stokes equations typically with the standard K-ε turbulence model on a three-dimensional almost general non-orthogonal grid using finite volume method. A control volume method is used for the discretization, together with the power-law scheme or the second order upwind scheme. The SIMPLE method is used for pressure coupling. The model is usually utilized for river engineering, environmental engineering, hydraulics, and sediment transport applications. Later, its utilization was extended to other hydraulic applications. The main advantage of SSIIM model over other computational fluid dynamic programs is its ability to model sediment transport in a live bed at complicated geometries [31]. The Navier–Stokes equations are following equations for in compressible fluid in vector mode.

$$\frac{\partial U_i}{\partial t} + U_j \frac{\partial U_i}{\partial Xi} = \frac{1}{\rho} \frac{\partial}{\partial X_i} (P\delta_{ij} - \rho \overline{u_i u_j}) \tag{4}$$

At above equation the first term on left is the time changes and the next term is displacement. The first term on the right is the pressure and the next is Reynolds stress. In order to assess the last term, a turbulence model is needed. In summary, we can know the equation of flow in turbulence model as a continuity equation and momentum equations. If it is supposed that the flow is steady $\left(\frac{\partial}{\partial_t} = 0\right)$ and the fluid is supposed incompressible, the momentum and continuity equations are explainable in following order.

$$\frac{\partial}{\partial xj}\left(\rho u_i u_j\right)=-\frac{\partial p}{\partial xj}\delta_{ij}+\frac{\partial}{\partial xj}\mu\left(\frac{\partial u_i}{\partial xj}+\frac{\partial u_j}{\partial xj}\right)+\frac{\partial}{\partial xj}\left(-\rho\overline{u_i}\,\overline{u_j}\right) \quad (5)$$

$$\frac{\partial}{\partial xj}\left(\rho u_j\right)=0 \quad (6)$$

That u_i and u_j are the parameter of velocity, ρ is the fluid density and P is the total pressure. According to upper equations, you can write three momentum equation and one continuity equation which three are totally 10 unknown (velocity on three sides *u*, *v*, *w* and six parameter of Reynolds stress) in them which means that the number of unknowns are more than the number of equations and in order to solve them you should use turbulence equation [31].

2.3.2. Numerical procedures

The channel was simulated in the SSIIM model exactly similar to the laboratory model. By comparing the results of the numerical model and the experimental one, the numerical model was validated and verified.

By running the SSIIM numerical model a set of networks or reading input files called KOORDINA (Network coordinates) and CONTROL files (Program control information) were created. The first step before mathematical modelling is discretizing the domain to cells where governing differential equations for flow and sediment fields shall be solved. Different meshes with various sizes were tested based on the sensitivity analysis results of meshing to simulate the 90° convergent bend. The field geometry has been defined in such a way that, the mesh size was decreased near the bridge pier, channel sidewall and inside the bend where the higher gradient existed. The mesh of other parts such as the straight sections of upstream and downstream of the channel was also considered coarser. Moreover, with the aim of reducing the computational time, the finer meshes were used in the flow direction approaching the bend. Overall, the meshes were assumed with dimensions of 30×20 mm and 10×20 mm in the straight sections of upstream and downstream of the channel, respectively. Also, in the bend section and around the pier, 10×10 mm meshes were used. Furthermore, in all cases, 11 meshes with the same spacing were used in the vertical direction. Eventually, the coordinates of the channel geometry were recorded in the koordina file.

In this study, about 25 different mesh sizes and configurations were tried in the numerical model design. Figure 5 shows a schematic view of the grids used in the numerical model. Although decreasing the mesh size increased the program runtime, but more accurate results were obtained. Also, some instability and divergence were seen in the program execution due to small meshes.

Other parameters, including the hydraulic conditions of the flow and sediment, the boundary conditions, the roughness coefficient, the governing equation solving methods, the relaxation coefficients, etc. were introduced in the control file. The simulation process starts with calibration of the model and calling the files of Koordina and control file by SSIIM model. After completing the calculations, simulation results such as speed components, shear stresses, water surface level and the maximum scour depth in the RESULT file were saved. In the following, we used the TECPLOT software (version EX 2015 R1) to plot and display different contours. In order to calibrate the SSIIM model, a range of the above-mentioned parameters were assigned to the software, and after numerous runs, the most consistent parameters between the numerical and experimental models were selected and used in other cases.

3. Results and discussion

In all experiments, it was observed that after the flow collision with the pier, the scouring rapidly occurred around it. (Fig. 6). Experimental observations showed that the scour hole around the pier is a function of the pier position in the bend, discharge rate, and the convergence rate. Results were recorded in different positions as shown in Table 2.

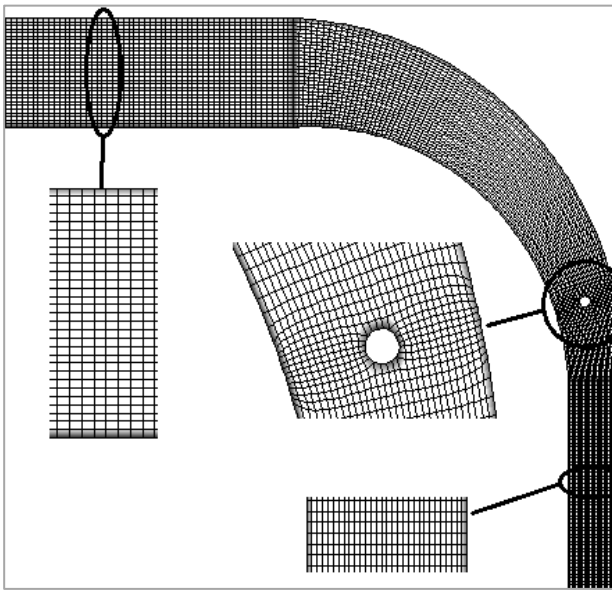

Figure 5. Grid sample used in the numerical model

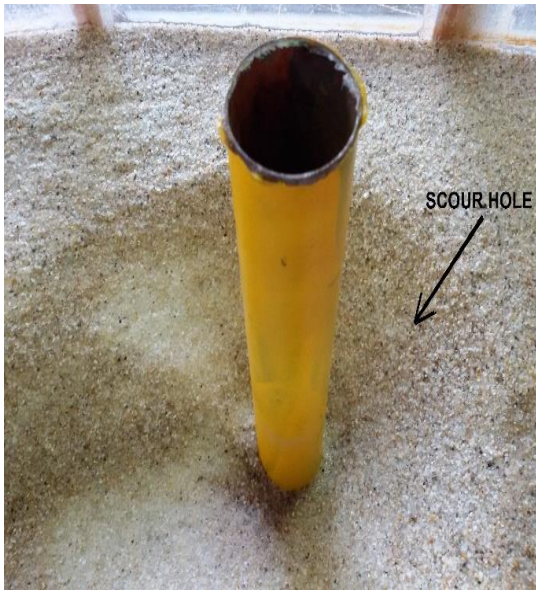

Figure 6. Scour pattern around cylindrical pier at the end of a test

Table 2. The results of maximum scour depth around cylindrical pier in different positions

Degree / Discharge of flow	0	30	45	65	75
Q=6.10 L/S & Fr=0.1	1.4	1.45	1.7	2.1	2.7
Q=8.23 L/S & Fr=0.14	1.65	2.00	2.3	3.8	5.1
Q=11.20 L/S & Fr=0.19	2.1	3.2	5.3	6.2	7.85

3.1. transverse profile of the scour hole around pier

Figure 7 indicates the comparison of dimensionless transverse profiles of the scour hole through the centerline of the cylindrical pier in positions (angles) of 0, 30, 45, 60, and 75 degrees for Froude number of 0.19 in both experimental and numerical models. In the first half of the bend (angles of 0, 30, and 45 degrees), little scour depths were seen and development of transverse profiles were fewer. It happened due to the bigger width of the channel and the weakness of the secondary currents in this region. By increasing the position in the second half of the bend (angles of 60 and 75 degrees), scour depths and development of the transverse profile increased, so that, the transverse profile extended out of symmetry toward the inner bend. Figure 7(a), depicts the status of the scour transverse profile at an angle of 0° and in both

numerical and experimental models. It is observed that in the experimental model, scour transverse profile extends at 33% of the bend's width, equivalent to 5 times the pier diameter, while, at the same location, scour occurs at 35% of the bend's width in the numerical model. It is clear that transverse profile is symmetric in both models and have a good agreement with errors of less than 6%.

As shown in figure 7(b), scour occurs beyond 47% of the bend's width and with the maximum depth occurring at a value of 2 cm at 30° and in experimental model. These values for the numerical model are 55 % and 2.6 cm, respectively. The error rate between the numerical and experimental models is estimated at about 25% in this position.

Figure 7(c) shows, when pier is located at position of 45°, the transvers profile does not extend significantly and it is approximately similar to the one with angle of 30°, but scour depth has increased remarkably. This can be due to the low convergence of bend and increasing shear stress around the pier in this area. Length of the transverse profile is 27.10 and 26.20 cm, equivalent to 60.22% and 58.20% of the bend's width in experimental and numerical model, respectively. On the whole, at the same location and in experimental model, maximum depth of transverse profile has increased by about 65% and 31% compared to angles of 0 and 30 degrees, respectively. Same comparison for numerical model shows an increase of about 45 and 50 percent, respectively.

For greater positions in the second half of the bend (angles of 60 and 75 degrees), it can be seen that (Figs. 7(d) and 7(e)), despite the reduction in bend's width, scour transverse profile is widened. This can be due to the high intensity of the secondary currents and greater convergence of bend in this region. Experimental observations and numerical results showed that increasing convergence and pier position in the bend leads to continuity between flow lines and shear stress intensity increase, respectively. On the other hand, synchronous effect of these two parameters also produces an increment in velocity of the flow collision with pier and a significant expansion of the scour hole. Figure 7(d) indicates that at an angle of 60°, scour has expanded to more than 86% of the channel width in both models, and the maximum scour depth is 5.8 and 5.4 cm in experimental and numerical models, respectively.

Figure 7(e) shows the status of the scour transverse profile at 75° angle in both experimental and numerical models. It can be seen from figure 7(e), with reaching the end of the bend at angle of 75°, the scouring reaches to its maximum value and the transverse profile has stretched all along the channel width. It is observed that in both experimental and numerical models, transverse profile expands up to 98% of the channel width. Moreover, at the same location, the maximum scour occurs at a value of 6.8 and 7.3cm, equal to 1.13 and 1.22 times the pier diameter in experimental and numerical models, respectively. According to figure 7, it is clear that, transverse profiles have a good agreement in both experimental and numerical models.

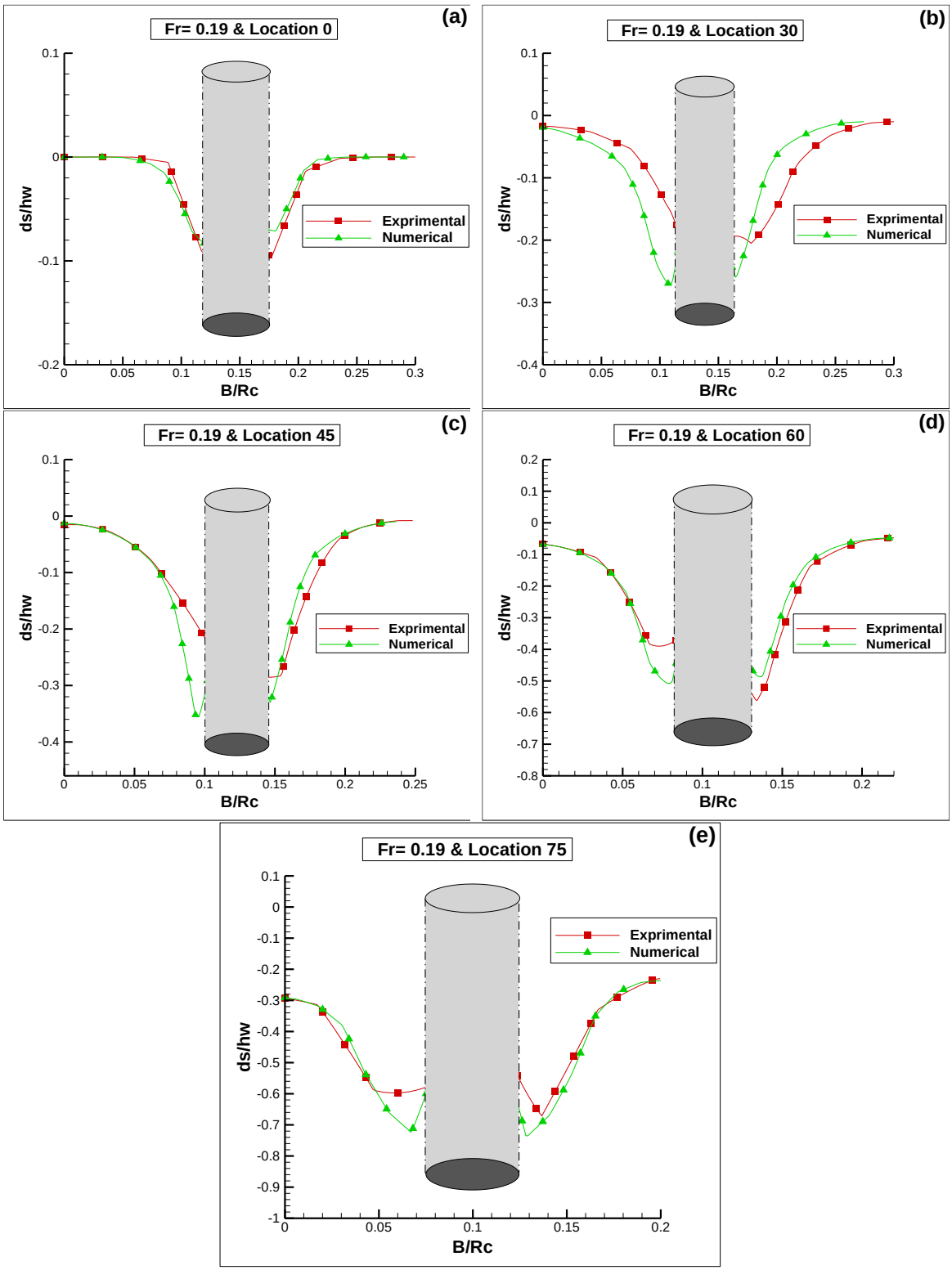

Figure 7. comparison of dimensionless transverse profiles of scour hole around pier in different positions, (a) location 0°, (b) location 30°, (c) location 45°, (d) location 60°, (e) location 75°

3.2. Scour hole around pier in different positions

Laboratory observations showed that installing the pier in different positions in the 90° convergent bend and the rate of bend convergence provide changes in bed's topography, depth, dimensions and volume of the scour hole around pier.

Scour hole geometry around cylindrical pier in positions of 0, 30, 45, 60, and 75 degrees under Fr=0.19 is shown for experimental and numerical models in Figures 8 and 9, respectively. As can be seen in Figures 8 and 9, by increasing the pier position in bend, the maximum depth and volume of the scour hole around pier are increased, but the geometry of scour hole is different and depends on the flow intensity and rate of the bend convergence. Observations also showed that in a wider section of the channel at primary angles of the bend, the difference between the transverse pressure gradient and the centrifugal force is low. This balance between pressure gradient and centrifugal force decreased the intensity of the secondary and helical currents in this area.

Figures 8(a) and 9(a) illustrate the geometry of scour hole at o° angle in experimental and numerical models, respectively. As it is obvious from Figures 8(a) and 9(a), scour hole is relatively symmetrical due to the wide section of the channel as well as the weakness of the secondary currents in both models. Figures 8(a) and 9(a) also show that, horseshoe vortices are less intense around pier and mainly form in front and upstream of the pier. It is clear that they do not have enough power to penetrate the back and downstream of the pier. Form Figures 8(a), it can be seen that, in the experimental model, the maximum scour depth is 2.1 cm, equivalent to 35% of the pier diameter, and volume of the scour hole is 0.00063 m3. On the other hand, in the numerical model, maximum scour depth is 1.8 cm, equivalent to 30% of the pier diameter and volume of the scour is estimated at 0.00057 m3 (Fig. 8(b)). It should be noted that the maximum scour depth occurred at front and vertex pier in both models. According to Figures 8(a) and 9(a), the maximum scour depth obtained in both models have a good agreement with errors of less than 14%. Figures 8(b) and 9(b) show that by entering to angle of 30 degrees, intensity of the shear stresses and volume of scour hole increase compared to angle of 0. As can be seen from figures, in this position the horseshoe vortices extend up to center of the pier. The maximum scour depth is 3.2 and 3.00 cm in experimental and numerical models, respectively. On the other hand, the volume of scour hole at angle of 30 degrees and for experimental and numerical models is estimated to be 0.0022 and 0.0019 m3, respectively. It should be noted that in this location and in both models the scour hole is almost symmetric. Figures 8(c) and 9(c) display the scour hole at 45° angle and in experimental and numerical models, respectively. From Figures (8(c) and 9(c)) it is observed, when pier is located at 45° angle, scour hole is gone out of symmetry mood and it is gradually stretched towards the inner bend. This can be due to the increased secondary currents and convergence rate relative to angles of 0 and 30 degrees. It is clear from Figures (8(c) and 9(c)) that at 45°, the geometry of scour hole around pier is not similar to the angles of 0 and 30 degrees. It is also observed that at angles of 0 and 30 degrees, the shape of scour hole is symmetrical and circular, while at 45°, the scour hole is more elongated and shaped like a bean around the pier. As can be seen in Figure 8(c), in the experimental model, the maximum depth and volume of scour hole are 5.3 cm and 0.001 m3, respectively. The same values for numerical model are 4.3 cm and 0.0013 m3, respectively (Fig. 9(c)).

By entering the second half of the bend (angles of 60 and 75 degrees), it was found that increasing the pier position in the bend and the rate of convergence had a significant effect on

local scour around the pier, so that scour reached its maximum value (Figs. 8(d,e) and 9(d,e)). Experimental observations showed that, increasing pier position in the bend led to an imbalance between pressure gradient and centrifugal force. Following this imbalance, secondary currents and shear stresses around pier increased. On the other hand, increasing convergence in bend led to increasing continuity between the flow lines. Those severe and numerous vortexes of horseshoe and wake formed around the pier were produced due to shear stresses and continuity of flow lines in the region and collision with the pier, so that surrounded all around the pier. According to Figures 8(d, e) and 9(d, e) it is observed that in second half of the bend, maximum scour depth is occurred in upstream and around the pier. According to Figure 8(d), it is seen that in the experimental model, maximum scour depth is 6.2 cm equivalent to 1.03 times the diameter of the pier at angel of 60°. The same values for the numerical model are 5.7 cm and 0.95 times, respectively (Fig. 9(d)). On the other hand, the maximum volume of hole in the laboratory and numerical models is 0.0028 and 0.0025 m3, respectively. Figures 8(e) and 9(e) depict the situation of the scour hole around the pier at an angle of 75 ° and in both experimental and numerical models, respectively. As can be seen in figures, in both models, the severity of the shear stresses and horseshoe vortexes have been increased dramatically and widely. It is also observed that the total width of the channel is strongly affected by these stresses, and the scour hole extends to the channel walls. It should be noted, due to the severity of the shear stresses in this position, the pier was vulnerable to falling. Generally, by reaching the end of the bend and at angle of 75°, the intensity of the secondary currents and horseshoe vortexes reached their maximum, so that, the maximum depth and volume of scouring hole occurred in this position. According to Figures 8(e) and 9(e), the maximum depth and volume of scouring hole in the laboratory model and at 75° were equal to 7.8 cm and 0.0037 m3, respectively. The correspondent values for the numerical model were equal to 7.57 cm and 0.0043 m3, respectively.

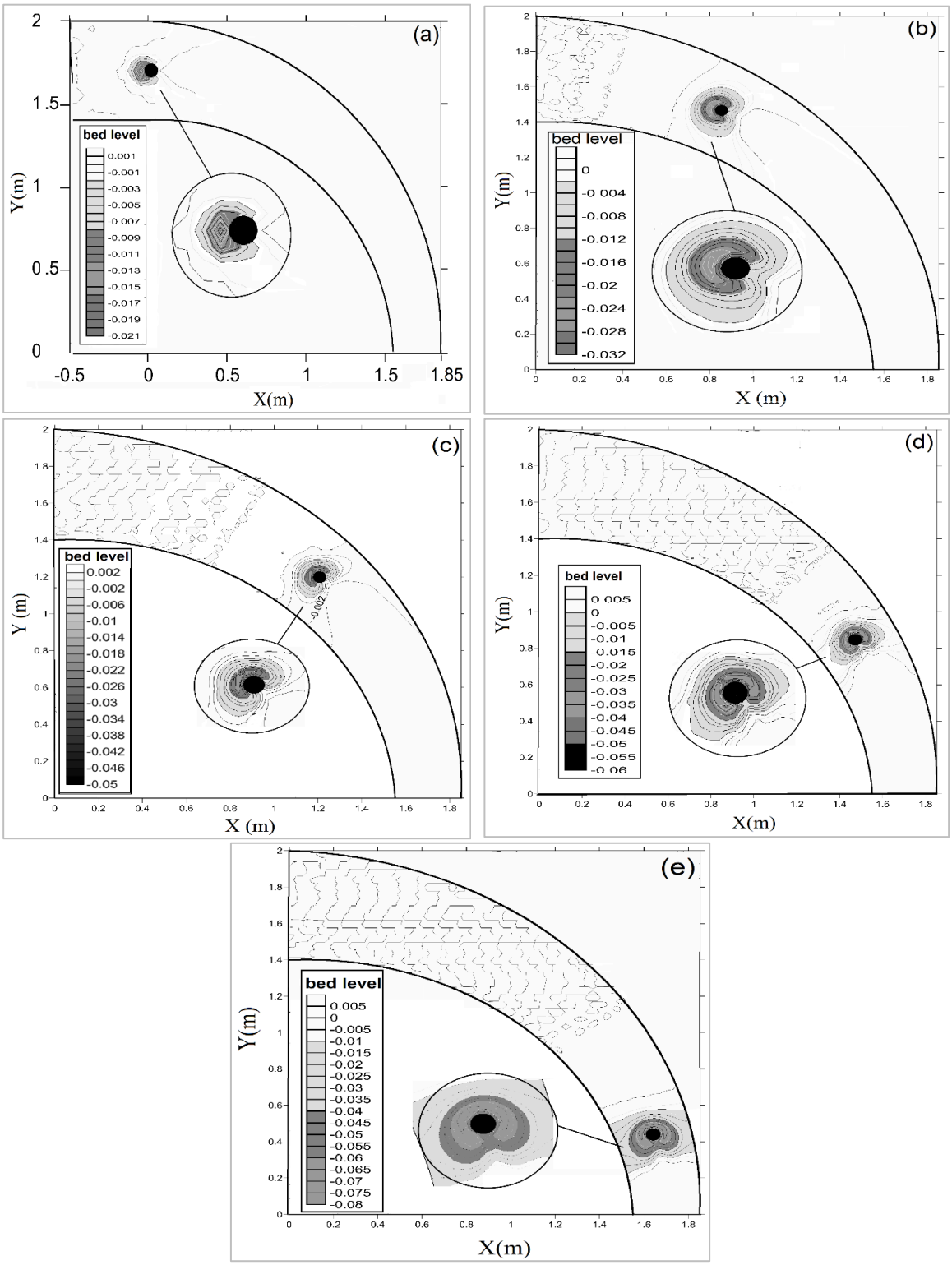

Figure 8. Scour hole around pier in different positions under fr=0.19 for experimental model. (a) location 0°, (b) location 30°, (c) location 45°, (d) location 60°, (e) location 75°

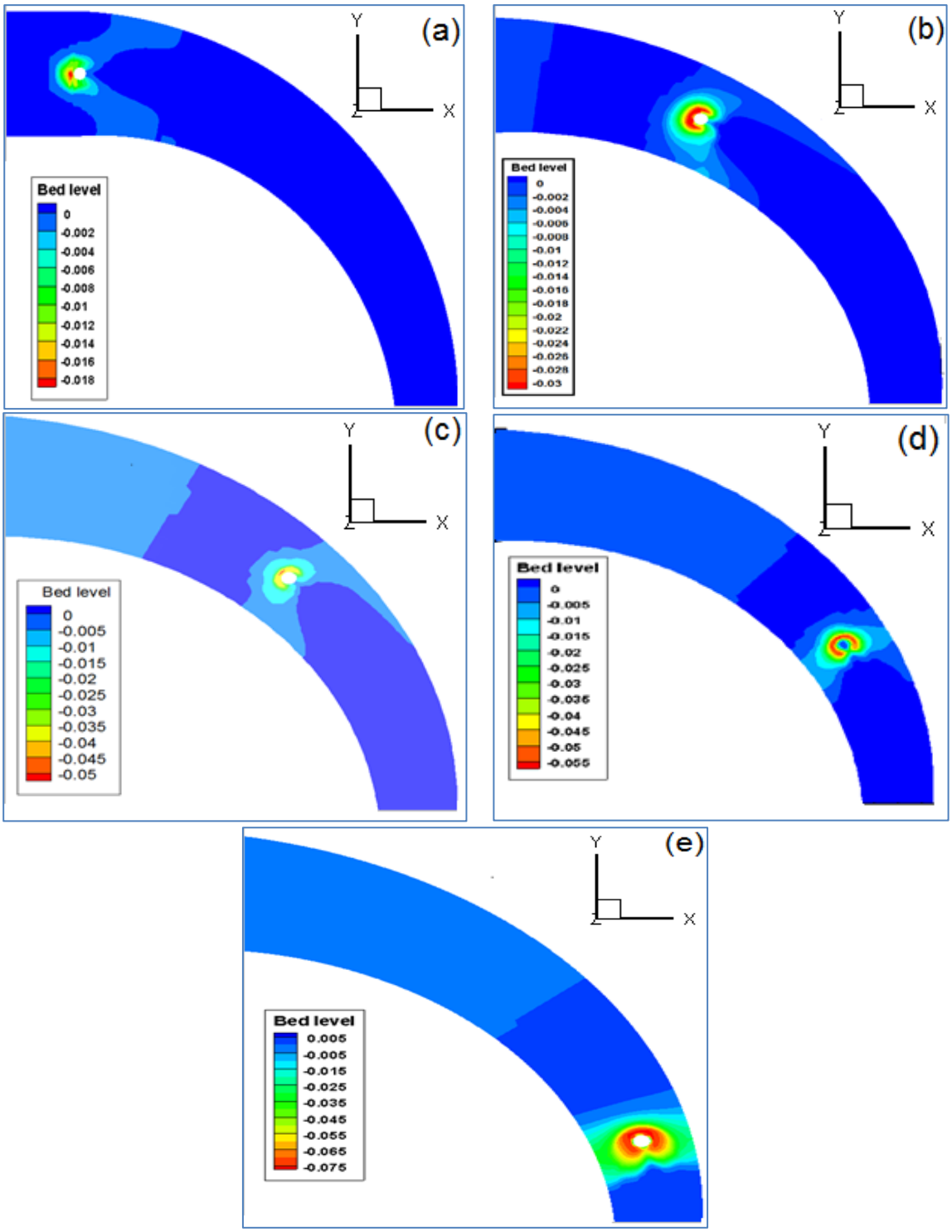

Figure 9. Scour hole around pier in different positions under fr=0.19 for numerical model. (a) location 0°, (b) location 30°, (c) location 45°, (d) location 60°, (e) location 75°

Figure 10, displays the changes of maximum scour depth around the cylindrical pier in different positions for Fr=0.19 in both experimental and numerical models. As can be seen, the maximum scour depth has a direct relation to pier position, so that by increasing the pier position in convergent bend, the maximum scour depth increases. The graph of Figure 10 shows that by changing the pier position from 0° at the beginning of the bend to 75° at the end of the bend, the maximum scour depth increases up to 74 % and 72% in experimental and numerical models, respectively. On the other hand, it can be seen that the maximum scour depth obtained from laboratory work and numerical model have a good agreement with errors of less than 3.33%, 6.25%, 16.98%, 6.45%, and 3.2% at angles of 0, 30, 45, 60, and 75 degrees, respectively.

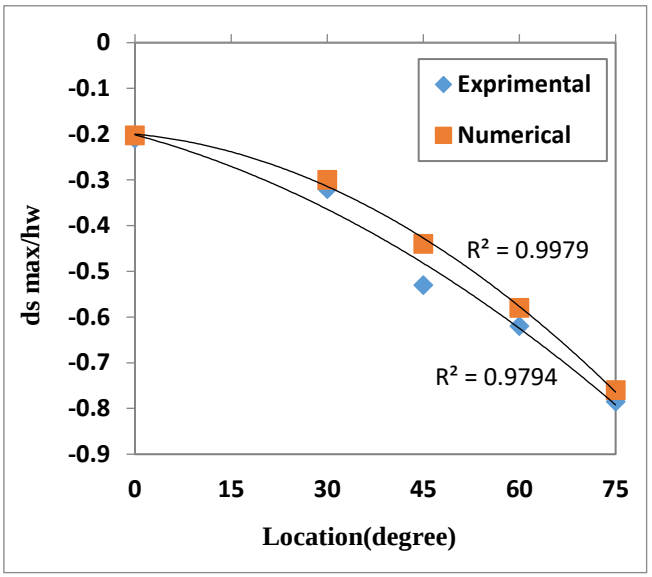

Figure 10. Changes of maximum scour depth in both models

Using all data sets used in this study, Figure 11 is plotted. It presents the comparison of experimental and numerical values relative to the maximum scour depth with regression coefficient of R2=0.9814. According to this Figure, it is obvious that there is a small scatter between these variables. It is also observed that, there is an acceptable agreement between the measured data in laboratory and the calculated values of the numerical model.

The changes of maximum scour volume around the cylindrical pier in different positions for Fr=0.19 in both experimental and numerical models is shown in Figure. 12. As it is shown, the maximum scour volume is increased proportional to the increment in pier position and convergence rate. According to Fig. 12, it can be seen that by changing the pier position (from 0° to 75°) and increasing the convergence rate by 58% (i.e. decreasing the bend's width by 58%), the maximum scour volume in the experimental and numerical models is increased by 487% and 654%, respectively.

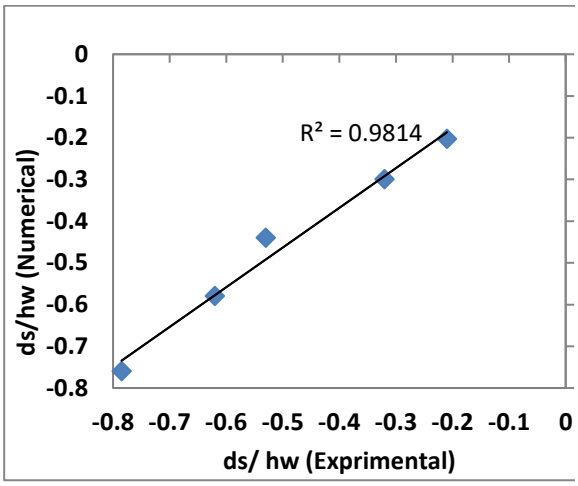

Figure 11. Comparison of maximum scour depth in both experimental and numerical models

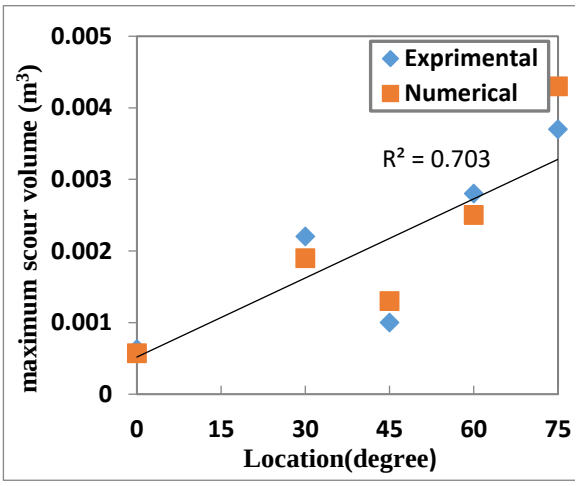

Figure 12. Comparison of maximum scour volume in both experimental and numerical models

3.3. Effect of flow discharge on maximum scour depth around the pier

One of the most effective parameters on local scouring around pier is the flow discharge rate or the Froude number. According to the continuity relation (Eq. (7)) the flow discharge rate has a direct relation with the velocity and cross-sectional area of the flow.

$$Q=A.V \tag{7}$$

In this research, Q stands for the flow discharge rate, A and V denote the cross-sectional area and velocity of the flow, respectively. Laboratory observations showed that by increasing flow discharge rate, the flow velocity is increased, so that, the horseshoe and wake vortexes are formed around the pier with more intensity. Furthermore, reducing the bend's width, especially in the second half of the bend (increasing the convergence at 60° and 75°), has a correlation with cross-sectional area of the flow reduction and subsequently, the intensity and velocity of the flow increased significantly. The observations showed that by increasing the flow rate, depth and volume of the scour hole around the pier reached its maximum value.

Figure 13 shows the comparison between the maximum scour depth around pier and changes of Froude number at positions of 0, 30, 45, 60, and 75 degrees in both experimental and numerical models. This figure shows that maximum scour depth is increased significantly by increasing Froude number, in both models. The calculations showed, with a 90% increment in Froude number, the maximum scour depth is increased up to 50%, 120%, 212%, 195%, and 190% in positions of 0, 30, 45, 60, and 75 degrees, respectively. Similarly, for the numerical model, maximum scour depth for the above-mentioned positions were obtained 190%, 130%, 175%, 190%, and 204%, respectively. The Figure 13 confirms the agreement between values of the maximum scour depth for both models in all cases.

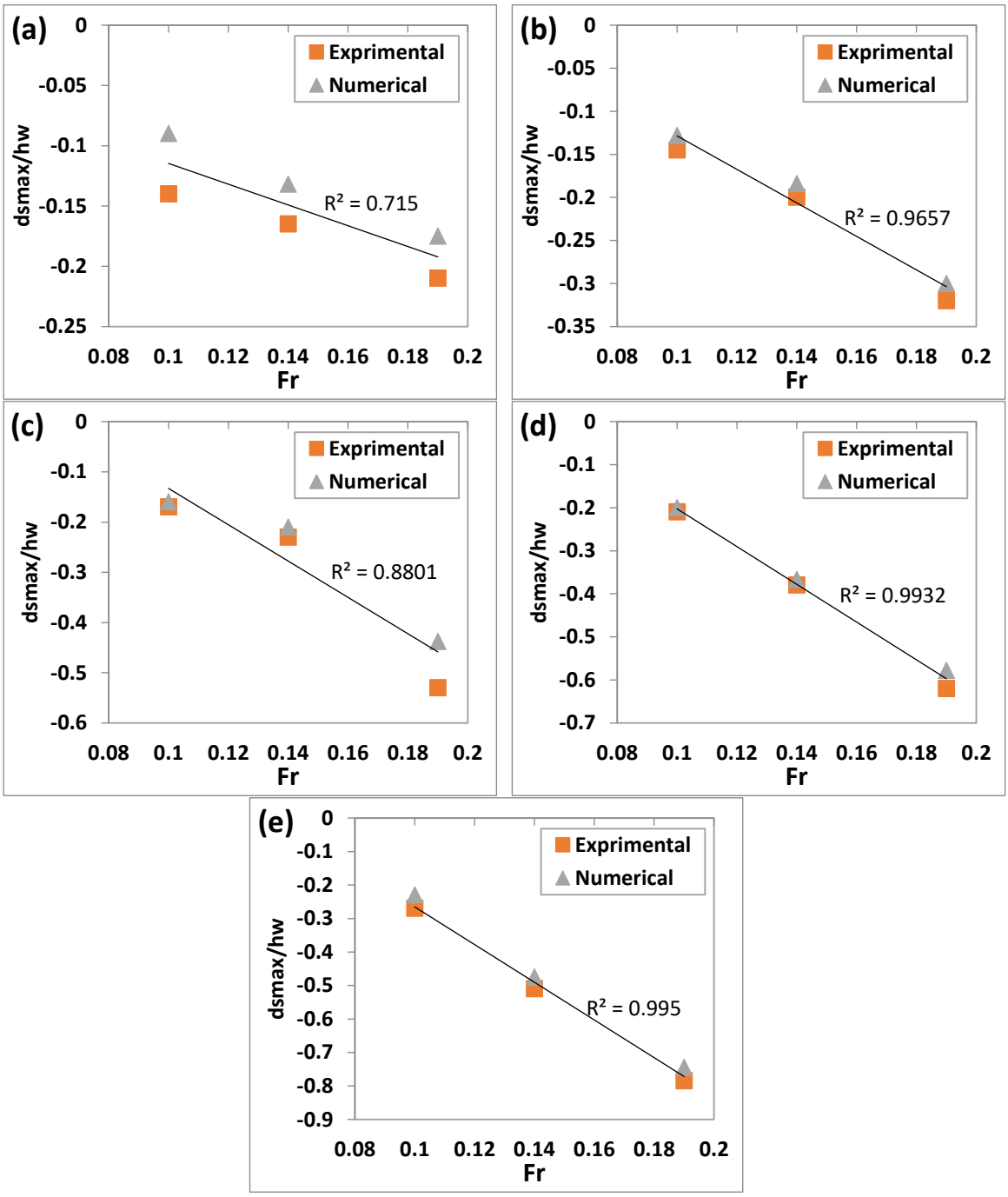

Figure 13. Comparison of maximum scour depth under different Froude numbers in experimental and numerical models. (a) Location 0°, (b) Location 30°, (c) Location 45°, (d) Location 60°, (e) Location 75°

3.4. Model performance evaluation

Table 3 shows the relative error of maximum scour depth values between experimental and numerical models in positions of 0, 30, 45, 60 and 75 degrees. The results show that the maximum scour depth values obtained from both experimental and numerical models are in good agreement, so that the maximum relative error is estimated at about 12% in position of 30 and under Froude number of 0.1. The validation errors are calculated as follows.

Table 3. Relative error of maximum scour depth between experimental and numerical models at different positions

Degree / Froude Number	ERROR%				
	0	30	45	60	75
Fr=0.1	11%	12%	6%	5%	11%
Fr=0.14	8%	8%	9%	3%	7%
Fr=0.19	7%	6%	8%	7%	5%

4. Conclusions

This study aimed to investigate the local scour around bridge pier located in a 90° convergent bend, experimentally and numerically. In particular, the effect of pier position in a convergent bend with flow discharge variations on the local scour was investigated. The results obtained from the experimental and numerical models were compared and based on discussion above, the following conclusions were deduced.

- Installation of pier in different positions and the rate of bend convergence brought the change in bed's topography, depth, dimensions and volume of scour hole around pier.
- Increasing the pier position in convergent bend led to increase intensity of secondary currents and shear stresses, so that maximum scour depth and volume of scour hole also increased.
- Increasing the convergence in bend increased the continuity between flow lines, and the composition of the horseshoe and wake vortices around the pier, so that maximum scour depth and volume of scour hole also increased.
- Simultaneous effect of convergence and increasing pier position, especially in the second half of the bend resulted in the extension of the scour hole up to the channel walls and significant increase in the scour depth around the pier.
- In all cases, the maximum depth and volume of the scour occurred in the second half of the bend at an angle of 75 degrees in both models.
- In all cases, minimum depth and volume of the scour occurred in the first half of the bend at an angle of 0 degrees in both models.
- Froude number is an important parameter and has a direct relation to scour, so that in all cases by increasing the Froude number, maximum depth and volume of the scour hole increased.
- In general, SSIIM numerical model efficiently simulates the position and value of the local scour around pier in a convergent bend, and the results obtained in the numerical case have a good agreement with the experimental results with low error percentage.

5. Acknowledgments

The authors thank all the staff of Islamic Azad University of Eghlid for providing the hydraulic lab.

6. Nomenclature

d_s	Maximum scour depth
L	Length of pier
b	width or diameter of pier
B	Width of channel
V	Velocity of flow
υ	Dynamic viscosity
∂	Temperature of flow
θ	Location of pier in bend
g	Gravitational acceleration
d_{50}	Median grain size
σ_g	Geometric standard deviation
Y	Flow depth
Or hw	
t	Equilibrium time of maximum scour depth
φ	Friction angle of sediment
ρ	Density of water
ρ_s	Density of sediment
Rc	Central radius of bend
S_0	Channel slope
$\frac{\vartheta}{vy}$	Effect of the viscous force (Reverse Reynolds number)
$\frac{gy}{V^2}$	Reverse Froude number
Fr	Froude number
Q	Flow discharge rate

7. References

1. Vijayasree BA, Eldho TI, Mazumder BS, Ahmad N, (2019). Influence of bridge pier shape on flow field and scour geometry. International Journal of River Basin Management, 17(1):109-129.
2. Rozovskii I.L., Flow of Water in Bend of Open Channels, Academy of Sciences of the Ukrainian SSR, Kiev, 1957.

3. Breusers H.N.C., Raudkivi A.J., Scouring. Hydraulic structures design manual, Balkema, Rotterdam, 1991.
4. Vaghefi M, Ghodsian M, Salimi S, (2016). The effect of circular bridge piers with different inclination angles toward downstream on scour. Indian Academy of Sciences (SADHANA), 41:75-86.
5. Shukry A, (1950). Flow around bends in an open flume. Transactions of the American Society of Civil Engineers, 15(1):751-779.
6. Booij R, (2003). Measurements and large eddy simulations of some curved flumes. Journal of Turbulence, 4(1):8-16.
7. Najafzadeh M, Barani GA, (2014). Experimental study of local scour around a vertical pier in cohesive soils. Scientia Iranica, Trans A, 21(2):241–250.
8. Blanckaert, K., Graf, W.H. (1999). Outer-bank cell of secondary circulation and boundary shear stress in open-channel bends. InProc. 1st RCEM symp, pp:533-543.
9. Wildhagen j., Applied Computational Fluid Dynamics with sediment Transport in a Sharply Curved Meadering Channel, Institute for Hydromechanics, Germany, University of Karlsruhe (TH), 2004.
10. Vaghefi M, Tabib Nazhad Motlagh MJ, Hashemi SSH, Moradi S, (2018). Experimental study of bed topography variations due to placement of a triad series of vertical piers at different positions in a 180° bend. Arabian Journal of Geosciences, 11(5).
11. Georgiadou AD, Smith KVH, (1986). Flow in curved converging channel. Journal of Hydraulic Engineering ASCE, 112(6):476-496.
12. Tabarestani MK, Zarrati AR, Mashahir MB, Mokallaf E, (2015). Extent of riprap layer with different stone sizes around rectangular bridge piers with or without an attached collar. Scientia Iranica. Transaction A, Civil Engineering, 22(3):709-716.
13. Ghodsian M, Mousavi SK, (2006). Experimental study on bed scour in a 90O channel bend. International Journal of Sediment Research, 21(4):321-328.
14. Ghobadian R, Mohammadi K, (2011). Simulation of subcritical flow pattern in 180° uniform and convergent open-channel bends using SSIIM 3-D model. Water Science and Engineering. 4(3):270-283.
15. Mansuri AR., 3-D Numerical Simulation of Bed Changes in 180 Degree Bends, M.S. Dissertation. Tarbyat Modares University, Tehran, Iran, 2006.
16. Gholami A, Akhtari AA, Minatour Y, Bonakdari H, Javadi AA, (2014). Experimental and numerical study on velocity fields and water surface profile in a strongly-curved 90° open channel bend. Engineering Applications of Computational Fluid Mechanics (EACFM), 8(3):447−461.
17. Abdallah Mohamed Y, Mohamed Abdel-Aal G, Hemdan Nasr-Allah T, Shawky A, (2016). Experimental and theoretical investigations of scour at bridge abutment. Journal of King Saud University – Engineering Sciences, 28(1):32–40.
18. Akib SH, Basser H, Karami H, Jahangirzadeh A, (2014). Retrofitting of Bridge Piers against the Scour Damages: Case Study of the Marand-Soofian Route Bridge. World Academy of

Science, Engineering and Technology, International Journal of Civil, Architectural Science and Engineering, 8(1):56-60.
19. Ehteram M, Mahdavi Meymand A, (2015). Numerical modeling of scour depth at side piers of the bridge. Journal of Computational and Applied Mathematics. 280:68–79.
20. Hamidi A, Siadatmousavi SM, (2017). Numerical simulation of scour and flow field for different arrangements of two piers using SSIIM model. Ain Shams Engineering Journal, 9(4):2415-2426.
21. Emami, Y., Salamatian, S.A., Ghodsian, M. (2008). Scour at cylindrical bridge pier in a 180-degree channel bend. Fourth International Conference on Scour and Erosion, Tokyo, Japan, pp: 256-262.
22. Masjedi A, Bejestan MS, Kazemi H, (2010). Effect of Bridge Pier Position in a 180 Degree Flume Bend on Scour Hole Depth. Journal of Applied Sciences, 10(8):670-675.
23. Wang H, Tang H, Xiao J, Wang Y, Jiang S, (2016). Clear-water local scouring around three piers in a tandem arrangement. Science China Technological Sciences, 59(6):888-896.
24. Khajeh SBM, Vaghefi M, Mahmoudi A, (2017). The scour pattern around an inclined cylindrical pier in a sharp 180-degree bend: an experimental study. International Journal of River Basin Management, 15(2):207-218.
25. Raudkivi AJ, Ettema R, (1983). Clear-water scour at cylindrical piers. Journal of Hydraulic Engineering (ASCE), 109(3):339-350.
26. Melville BW, Sutherland AJ, (1988). Design method for local scour at bridge piers. Journal of the Hydraulics Division, 114(10):1210-1225.
27. Guemou B, Seddini A, Ghenim NA, (2016). Numerical investigations of the round-nosed bridge pier length effects on the bed shear stress. Progress in Computational Fluid Dynamics, 16(5):313-321.
28. Melville BW, Chiew YM, (1999). Time scale for local scour at bridge piers. Journal of Hydraulic Engineering ASCE, 125(1):59-65.
29. Oliveto G, Hager WH, (2002). Temporal Evolution of Clear-Water Pier and Abutment Scour. Journal of Hydraulic Engineering ASCE, 128(9):811-820.
30. Olsen NRB, Jimenes OF, Abrahamsen L, Lovoll A, (1999). 3D CFD modeling of water and sediment flow in a hydropower reservoir. International Journal of Sediment Research, pp.16-24.
31. Olsen, N.R.B., A three-dimensional numerical model for simulation of sediment movements in water intakes with multi block option, Online User's manual, 2011.

Formatting of funding sources

This research did not receive any specific grant from funding agencies in the public, commercial, or not-for-profit.